Fibers pre-treatments with sodium silicate affect the properties of suspensions, films, and quality index of cellulose micro/nanofibrils

Article *in* Nordic Pulp & Paper Research Journal · July 2022

DOI: 10.1515/npprj-2022-0037

CITATIONS
10

READS
392

8 authors, including:

Adriano Reis Prazeres Mascarenhas
Universidade Federal de Rondônia
90 PUBLICATIONS **218** CITATIONS
SEE PROFILE

Mário Scatolino
Universidade do Estado do Amapá - (UEAP)
78 PUBLICATIONS **849** CITATIONS
SEE PROFILE

Matheus Cordazzo Dias
Universidade do Estado do Amapá
44 PUBLICATIONS **412** CITATIONS
SEE PROFILE

Maria Alice Martins
Brazilian Agricultural Research Corporation (EMBRAPA)
83 PUBLICATIONS **1,969** CITATIONS
SEE PROFILE

Miscellaneous

Adriano Reis Prazeres Mascarenhas*, Mário Vanoli Scatolino, Matheus Cordazzo Dias, Maria Alice Martins, Rafael Rodolfo de Melo, Renato Augusto Pereira Damásio, Maressa Carvalho Mendonça and Gustavo Henrique Denzin Tonoli

Fibers pre-treatments with sodium silicate affect the properties of suspensions, films, and quality index of cellulose micro/nanofibrils

Effect of Na_2SiO_3

https://doi.org/10.1515/npprj-2022-0037
Received April 21, 2022; accepted July 8, 2022

Abstract: The characteristics of cellulose micro/nanofibrils (MFC/CNF) can be improved with pre-treatments of the original fibers. The present work is proposed to study pre-treatment with sodium silicate (Na_2SiO_3) on bleached fibers of *Eucalyptus* sp. (EUC) and *Pinus* sp. (PIN) and its effects on the quality index of MFC/CNF. Particle homogeneity, turbidity, and microstructure of the suspensions were evaluated. Similarly, the physical-mechanical, and barrier properties of the films were studied. With the results obtained for suspensions and films, the quality index (QI) was MFC/CNF calculated. The smallest particle dimension was observed for MFC/CNF of *Pinus* sp. with 10 % of Na_2SiO_3, as well as the lowest turbidity (~350 NTU) was obtained for MFC/CNF of *Pinus sp*. with 5 % of Na_2SiO_3. The pre-treatments reduced the transparency of the films by ~25 % for EUC and ~20 % for PIN. The films presented a suitable barrier to UVC radiation, water vapor, and oil. The tensile strength of EUC and PIN films was increased by 20 % using 10 % of Na_2SiO_3. The same concentration of Na_2SiO_3 provided QI 70 for EUC MFC/CNF. The Na_2SiO_3 was efficient to obtain the MFC/CNF with interesting properties and suitable to generate films with parameters required for packaging.

Keywords: biorefinery; cellulose nanofibrils (CNF); cell wall; microfibrillated cellulose (MFC); nanotechnology.

Introduction

Cellulose has been intensively studied to reduce the consumption of materials derived from petroleum through the development of new products because it is abundant, produced by renewable sources, biodegradable, and has great versatility. Among research developed with cellulose, studies on cellulosic nanomaterials (CNM) should be highlighted (Mokhena and John 2020). CNM includes bacterial cellulose (BC), cellulose nanocrystals (CNC), cellulosic nanofibrils (CNF), microfibrillated cellulose (MFC), and cellulose micro/nanofibrils (MFC/CNF) (Tayeb et al. 2018, Balea et al. 2020, Chanda and Bajwa 2021). Additionally, these materials attract interest from the scientific

***Corresponding author: Adriano Reis Prazeres Mascarenhas,** Department of Forest Engineering, Federal University of Rondônia (UNIR), 76940-000 Rolim de Moura, RO, Brazil, e-mail: adriano.mascarenhas@unir.br, ORCID: https://orcid.org/0000-0002-7554-3590
Mário Vanoli Scatolino, Department of Production Engineering, State University of Amapá (UEAP), 68900-070 Macapá, AP, Brazil; and Agricultural Sciences Center, Federal University of the Semiarid (UFERSA), 59625-900 Mossoró, RN, Brazil, e-mail: marioufla@posgrad.ufla.br, ORCID: https://orcid.org/0000-0002-0412-994X
Matheus Cordazzo Dias, Maressa Carvalho Mendonça, Gustavo Henrique Denzin Tonoli, Department of Forest Science, Federal University of Lavras (UFLA), C. P. 3037, 37200-900 Lavras, MG, Brazil, e-mails: matheus.cordasso@gmail.com, maressacmendonca@gmail.com, gustavotonoli@ufla.br, ORCID: https://orcid.org/0000-0002-8154-2543 (M. C. Dias), https://orcid.org/0000-0001-7532-7794 (M. C. Mendonça), https://orcid.org/0000-0002-6502-8974 (G. H. D. Tonoli)
Maria Alice Martins, Embrapa Instrumentation – National Laboratory of Nanotechnology for Agribusiness, 13561-206 São Carlos, SP, Brazil, e-mail: maria-alice.martins@embrapa.br, ORCID: https://orcid.org/0000-0002-6416-6929
Rafael Rodolfo de Melo, Agricultural Sciences Center, Federal University of the Semiarid (UFERSA), 59625-900 Mossoró, RN, Brazil, e-mail: rafael.melo@ufersa.edu.br, ORCID: https://orcid.org/0000-0001-6846-2496
Renato Augusto Pereira Damásio, Klabin – Technology Center, Fazenda Monte Alegre, Santa Harmonia, 03, 84275-000 Telêmaco Borba, PR, Brazil, e-mail: rdamasio@klabin.com.br, ORCID: https://orcid.org/0000-0001-7268-2774

and industrial community due to their properties such as biocompatibility, high surface area, three-dimensional microstructure, unique optical properties, high rigidity, and specific strength (Guan et al. 2020, Mokhena et al. 2021). Other research horizons of MFC/CNF refer to applications in optical and electrical sensors (Teodoro et al. 2021), drug and food encapsulation (Amalraj et al. 2018), paper coatings for packaging (Yook et al. 2020), film production and composite reinforcement (Mascarenhas et al. 2022), emulsion stabilizers (Li et al. 2021), and water treatment processes (Mohammed et al. 2018).

MFC/CNF are produced by chemical methods or processes based on mechanical shearing of fibers' cell walls. The most used mechanical processes include microfluidization (Perrin et al. 2020), sonication (Wu et al. 2021), high-pressure homogenization (Karina et al. 2020), and mechanical fibrillation in ultra refiner (Berto and Arantes 2019). Nevertheless, the energy demand for cell wall deconstruction is a limiting factor for MFC/CNF production in industrial scaling, as the consumption values range between 20000 kWh/t and 30000 kWh/t (Kumar et al. 2021).

Due to the high power consumption, enzymatic, mechanical, or chemical pre-treatments are applied to the fibers. Pre-treatments can also modify the cellulose surface, depending on the applications, such as carboxymethylation, silylation, cationization, phosphorylation, sulfoethylation, and TEMPO (2,2,6,6 – tetramethylpiperidine-1-oxyl) mediated oxidation (Rol et al. 2019, Trovagunta et al. 2021). Although pre-treatments can significantly reduce energy consumption, the reagent cost is high or the process results in the formation of chemical compounds harmful to health and the environment, as observed in TEMPO-mediated oxidation.

Alkaline pre-treatments are studied as an alternative to reduce energy consumption and reagent costs for MFC/CNF production (Sukmawan et al. 2022). Alkaline agents enhance the MFC/CNF individualization because they promote fiber swelling, reduce the degree of cellulose polymerization and remove hemicelluloses by breaking intermolecular ester bonds with cellulose and lignin, enabling the gelation process (Noremylia et al. 2022).

The main alkaline pre-treatments are NaOH-based solutions in concentrations ranging from 2 % to 10 %. Martins et al. (2021) obtained MFC/CNF with diameters varying between 15 nm and 30 nm and observed a 48 % of reduction in energy consumption, using NaOH solution 5 % (m/m) as pre-treatment for unbleached *Eucalyptus* sp. fibers. Similarly, Dias et al. (2019) reduced energy consumption for MFC/CNF production by 40 % for *Eucalyptus* sp. and 62 % for *Pinus* sp. On the other hand, Malucelli et al. (2019) reported that the NaOH does not always reduce energy consumption and can impair the MFC/CNF quality, as the alkaline action can possibly make the fibers stiffer and reduce the colloidal stability. Limitations such as this indicates the need to research other alkaline pre-treatments. Sodium silicate (Na_2SiO_3) can be considered as an alternative for this purpose because of solutions with concentrations greater than 5 % (m/m) present pH between 12 and 14 (Hashem et al. 2010). Na_2SiO_3 solutions are applied to remove lignin and hemicelluloses to improve the cellulosic pulp bleaching (Moghaddam and Karimi 2020).

However, the effects of Na_2SiO_3 on MFC/CNF suspensions and derivatives (foam, films, nanopapers, and composites) are little-known and may influence the characteristics of turbidity, transparency, barrier, and mechanical properties, making them different from those obtained by more conventional pre-treatments. Therefore, studies aiming to compare MFC/CNF obtained by different processes and pre-treatments are essential to facilitate decision-making regarding their applications. Desmaisons et al. (2017) developed a quality index using multivariate models with high precision based on characterizations of MFC/CNF in a simplified way. This index is calculated from the properties obtained from the suspension (turbidity, particle homogeneity, and macroscopic dimension) and MCF/CNF films (Young's modulus, porosity, and transmittance).

The research amount using this methodology is incipient, due to the fact of being a relatively new method, as we can see in works such as Desmaisons et al. (2018), Rol et al. (2018), Banvillet et al. (2021a), Banvillet et al. (2021b) and Espinosa et al. (2020). As the database on MFC/NFC produced from pre-treatments with Na_2SiO_3 is very scarce, the present work proposed to evaluate the pre-treatments of *Eucalyptus* sp. (EUC) and *Pinus* sp. (PIN) pulps with Na_2SiO_3 solutions at concentrations of 5 % and 10 % (*m*/*m*) and its effects on the properties of the suspensions, films, and MFC/NFC quality index.

Materials and methods

Fibers pre-treatment with sodium silicate

Commercial bleached kraft pulps of *Eucalyptus* sp. (EUC) and *Pinus* sp. (PIN) were subjected to pretreatment with Na_2SiO_3 (18 % Na_2O; 63 % SiO_2) produced by Dinâmica Química LTDA (São Paulo, Brazil). Na_2SiO_3 solutions with concentrations of 5 % and 10 % (m/m) (Table 1) were prepared with deionized water heated in a water bath at a tem-

Table 1: Identification of pre-treatments with sodium silicate solutions in different concentrations applied to fibers from *Eucalyptus* sp. and *Pinus* sp.

Pulp	Condition	Identification
Eucalyptus sp.	Untreated	*EUC control*
	Pre-treatment with 5 % of Na_2SiO_3	*EUC SS 5 %*
	Pre-treatment with 10 % of Na_2SiO_3	*EUC SS 10 %*
Pinus sp.	Untreated	*PIN control*
	Pre-treatment with 5 % of Na_2SiO_3	*PIN SS 5 %*
	Pre-treatment with 10 % of Na_2SiO_3	*PIN SS 10 %*

perature of 80 °C. After solubilization, EUC and PIN pulps were mixed with Na_2SiO_3 solutions to obtain suspensions of 2.5 % consistency (m/m). Pulps were kept at a temperature of 80 °C ± 2 °C and constant stirring of 500 rpm for 2 h (Dias et al. 2019), being posteriorly washed in deionized water until pH 7.

Production of cellulose micro/nanofibrils suspensions and films

Suspensions with pre-treated fibers in 2.0 % (w/w) for EUC and 1.5 % (w/w) for PIN were produced using deionized water. To ensure swelling and dispersion, the fibers were stirred at 500 rpm for 15 min. Suspensions with untreated fibers in the same proportions presented were also produced. The fibrillation process was carried out with 5 passes of suspensions through the grinder – Supermass-colloider Masuko Sangyo MKGA-80 (Kawaguchi, Japan), at 1500 rpm. The initial distance between the grinder discs was 10 µm and was adjusted to 100 µm as the suspension viscosity increased. The energy consumptions of fibrillation were 3000 kWh/t for *EUC SS 5 %*, 4100 kWh/t for *EUC SS 10 %*, 4000 kWh/t for *PIN SS 5 %* and 4500 kWh/t for *PIN SS 10 %*. For untreated fibers, energy consumption was 7500 kWh/t for EUC and 10000 kWh/t for PIN until gel formation. Films were produced with MFC/CNF suspensions in the concentration of 1 % (w/w) by the "*casting*" method, which consists of solvent evaporation at room temperature (± 22 °C). Each film was produced from 50 g of suspension poured into acrylic plates with a diameter of 15 cm. Five films were produced for each treatment.

Chemical characterization of the fibers

Contents of extractive-free carbohydrates of treated and untreated EUC and PIN fibers were determined following the TAPPI T 249 cm 21 standard (TAPPI 2021a). Lignin content was obtained according to the procedure described in TAPPI T 222 om-02 (TAPPI 2021b). For both pulps, cellulose content was calculated by subtracting the total glucose content and the glucose content associated with mannose, since for every 3 mannose units there is one glucose unit (Dias et al. 2019). Therefore, hemicellulose content was obtained by the sum of galactose, arabinose, xylose, and mannose, with the respective glucose amount (Zhou et al. 2016, Qaseem et al. 2021).

Dimension and homogeneity of the particles

To estimate the fiber's residual fraction after the fibrillation process, images were taken using the Olympus BX41 light microscope (Tokyo, Japan). MFC/CNF suspensions were diluted in deionized water in proportion 0.1 % (w/w). Suspension drops were deposited on glass slides and covered with a coverslip for observation using an objective of 10x.

The images obtained were transformed into the 8-bit format and analyzed using the "particle analysis" routine to obtain the average area of particles (macroscopic dimension), of the software Image J (Rueden et al. 2017). This procedure was performed using six images per sample. Homogeneity of particles was calculated with the relative frequency observed for visible particles smaller than 5 μm^2, between 5 and 10 μm^2, and larger than 10 μm^2 (Desmaisons et al. 2017). As greater the number of particles included in the same size class, with a smaller standard deviation for each class, the greater the homogeneity.

Turbidity of the suspensions

The turbidity of the MFC/CNF suspensions was determined in a Plus Alfakit turbidimeter (Santa Catarina, Brazil), adjusted to a wavelength of 860 nm. MFC/CNF aliquots were collected, under stirring at 900 rpm, in concentration 0.1 % (w/w). Five measurements were done for each sample.

Microstructure of the films

Films samples with 5 × 5 mm were submerged in liquid nitrogen for instant freezing, then fractured and fixed on sample holders (stubs) containing double-sided adhesive tapes. The samples were subjected to metallic coating in a gold evaporator (SCD 050) before the micrographs obtainment in an ultra high resolution (UHR) scanning electron microscope with a field emission gun (SEM/FEG) TESCAN

CLARA (Libušina, Czech Republic), under the conditions of 10 KeV, 90 pA, with a working distance of 10 mm.

Physical properties of the films

Before the mentioned tests, the films were conditioned at a temperature of 25 °C and relative humidity of 65 %, according to TAPPI T 402 sp-21 (TAPPI 2021c). The thickness of the films was obtained using a digital micrometer (0.001 mm), following the TAPPI T 411 om-15 standard (TAPPI 2015). The grammage was obtained according to TAPPI T 410 om-08 standard (TAPPI 2013), weighing the films in analytical balance and determining their respective areas with a digital caliper (0.001 mm). The grammage (g/m^2) was calculated with the ratio mass/area. The bulk density of the films was calculated by the ratio between the grammage and thickness. The porosity (Φ) was calculated by the ratio between the bulk density of the film and the cellulose density (Equation (1)).

$$\Phi(\%) = 1 - \left(\frac{\rho f}{\rho c}\right) \tag{1}$$

where ρf is the bulk density of the films (kg/m^3) and ρc is the cellulose density (1540 kg/m^3).

Light transmittance and transparency of the films

The light transmittance on the films was obtained in five replications for each treatment, in a Genesys 10S UV-Vis Thermo Scientific spectrophotometer (Massachusetts, USA), adjusted with wavelength ranging between 200 and 800 nm. The transmittance obtained at 600 nm was used to calculate the transparency of the films (Tr), following the procedures presented by Sothornvit et al. (2010) (Equation (2)). The transmittance observed in 550 nm was used to calculate the quality index.

$$\mathrm{Tr}(\%) = \frac{(\log T_{600})}{\mathrm{th}} \tag{2}$$

where T_{600} = transmittance in 600 nm (%) and th = thickness of the films (mm).

The opacity of the films was obtained following the methodologies presented in Fakhouri et al. (2013) and Lago et al. (2020). A Konica Minolta CM-5 colorimeter (Osaka, Japan), adjusted with a viewing angle of 10 ° and D65 illuminant (daylight) was used for the analysis. For obtaining the luminosity values (L^*), the films were evaluated in a black pattern and a white one. These data were used to calculate the apparent opacity (Equation 3) and the results were expressed on a scale from 0 to 100 %. For each treatment, five samples were analyzed.

$$\mathrm{Opacity}(\%) = \frac{Yb}{Yw} \times 100 \tag{3}$$

where Yb = sample luminosity in the black pattern and Yw = sample luminosity in the white pattern.

Water vapor barrier and grease resistance of the films

Five samples with a diameter of 16 mm were prepared for each treatment and stored in a conditioned room with a temperature of 25 °C and relative humidity of 65 % for three days, according to ASTM E96-16 (ASTM 2016). After this period, the samples were placed in glass capsules partially filled with dry silica. The capsules were placed in desiccators containing saturated KCℓ solution at 38 °C to create an atmosphere with a relative humidity of 90 %, as requested by ASTM E104-02 (ASTM 2012). The capsules with samples were weighed in analytical balance for eight consecutive days. The water vapor transmission rate (WVTR) and water vapor permeability (WVP) were calculated with Equation (4) and Equation (5).

$$\mathrm{WVTR}(\mathrm{g/m^2\,day}) = \frac{\mathrm{W}}{t \times A} \tag{4}$$

$$\mathrm{WVP}(\mathrm{g\,mm/kPa^{-1}\,day\,m^2}) = \frac{(\mathrm{WVTR} \times \mathrm{th})}{(p \times \mathrm{UR}_o - \mathrm{UR}_i)} \tag{5}$$

where W = capsule weight with sample (g); t = time (days); A = exposed area of sample (m^2); th = film thickness (mm); p = water vapor pressure (kPa); UR_o and UR_i are, respectively, the the humidity inside the desiccator (90 %) and inside the capsule.

A grease resistance test was conducted following the TAPPI T 559 cm-12 standard (TAPPI 2012). Ten films with dimensions 216 × 279 mm were cut, in which drops of the test solutions were applied. The solutions were classified from 1, less aggressive and composed only of oil, to 12, more aggressive and composed of toluene and *n*-heptane. One drop of oily solution was applied on the film surface, being removed after 15 s. The film was classified with the highest score (solution from 1 to 12) that permeates the sample.

Mechanical properties of the films

The tensile strength of the films was evaluated according to ASTM D 882-18 (ASTM 2018) using a Stable Micro Sys-

tems texturometer, TATX2i, (England, United Kingdom) equipped with a load cell with a capacity of 500 N. To determine the tensile strength, Young's modulus, and elongation at break, 10 specimens were tested for each treatment, with dimensions of 10 × 100 mm. The initial distance between the grips was 50 mm, with a test speed of 0.8 mm/s.

Quality index of the cellulose micro/nanofibrils

The simplified quality index (QI) was determined from the multivariate model developed by Desmaisons et al. (2017), using data of macroscopic dimension, particle homogeneity, turbidity, the transmittance at 550 nm, Young's modulus, and porosity (Equation (6)). The parameters "weights" applied must result in the sum of 10. Therefore, the distribution of weights was carried out according to the application (films for packaging and colloidal stabilizers) of suspensions and films reported in the literature (Desmaisons et al. 2018, Rol et al. 2019).

$$\begin{aligned} QI = {} & 1.5 \times [-2.67 \times \ln(x_1) + 12.81] + 1.5 \times [0.18 \times (x_2)] \\ & + 1.5 \times [0.10 \times (x_3) + 11] + 1.5 \times [1.65 \times \ln(x_4) + 2.7] \\ & + 1.5 \times [-0.036 \times (x_5) \times 1.27 \times (x_5)] \\ & + 2.5 \times [3.81 - 0.16 \times (x_6)] \end{aligned} \quad (6)$$

where x_1 = macroscopic dimension (μm^2); x_2 = homogeneity (%); x_3 = turbidity (NTU); x_4 = transmittance in 550 nm; x_5 = Young's modulus (GPa); and x_6 = porosity (%).

Statistical analysis

Data obtained were analyzed using descriptive statistics, using the software R Core Team (2020), indicating average and standard deviation.

Results and discussion

Chemical composition

Regarding *EUC control*, treatments *EUC SS 5 %* and *EUC SS 10 %* reduced hemicellulose contents by 2.6 % and 1.3 %, respectively, resulting in a slight increase in relative cellulose contents (Table 2). Compared with the *PIN control*, *PIN SS 5 %* obtained a reduction of 3.4 % in hemicelluloses amount, whereas for *PIN SS 10 %*, the reduction was 13.1 %. In addition, for PIN pulp, the type of hemicellulose most affected by the treatment with 10 % Na_2SiO_3 was mannose, followed by xylose and arabinose.

These results can be explained by the high Na_2SiO_3 solution alkalinity (pH ~ 12). Na_2SiO_3 is used to increase the capacity to remove lignin and hemicelluloses, improving the pulp bleaching (Hashem et al. 2010, Moghaddam and Karimi 2020). Studies indicate that hydrolysis of alkaline solutions promotes the saponification of intermolecular ester cross-links that link hemicelluloses to cellulose or other components such as lignin (Grigatti et al. 2015, Melati et al. 2019). Removing hemicelluloses from fibers promotes an increase in relative sugar content, allows easier access to cellulose chains, and facilitates cell wall swelling (Shimizu et al. 2016). These effects facilitate the MFC/CNF production by mechanical method, as the cell wall swelling promotes the macrofibrils loosening, increases the contact surface of fibers, making them more susceptible to shocks against the grinder stones, intensifying the shear forces on the cell wall (Trovagunta et al. 2021). With more passes through the grinder, the alkaline pre-treatments potentiate the reduction of particle sizes and increase the exposure of the cellulose OH groups. Further, there is an increase in the number of hydrogen bonds between cellulose and water, facilitating gelation (Fonseca et al. 2019). These mechanisms can reduce energy consumption during MFC/CNF production (Martins et al. 2021).

Table 2: Average and standard deviation for chemical components of untreated and pre-treated pulps with sodium silicate solutions in concentrations 5 % and 10 %.

Identification	Glucose	Galactose	Arabinose	Xylose	Mannose	Total lignin	Cellulose	Hemicelluloses
EUC control	79.1 ± 0.3*	ND**	ND	15.7 ± 0.1	ND	0.4 ± 0.1	79.1 ± 0.3	15.7 ± 0.1
EUC SS 5 %	80.2 ± 0.2	ND	ND	15.5 ± 0.2	ND	0.5 ± 0.1	80.2 ± 0.2	15.5 ± 0.2
EUC SS 10 %	80.1 ± 0.5	ND	ND	15.3 ± 0.3	ND	0.8 ± 0.1	80.1 ± 0.5	15.3 ± 0.3
PIN control	80.0 ± 0.7	ND	0.5 ± 0.1	9.6 ± 0.1	7.5 ± 0.1	0.5 ± 0.1	78.2 ± 0.6	17.6 ± 0.3
PIN SS 5 %	79.6 ± 0.2	ND	0.5 ± 0.1	9.4 ± 0.1	7.1 ± 0.1	0.7 ± 0.1	77.9 ± 0.3	17.0 ± 0.3
PIN SS 10 %	79.9 ± 1.1	ND	0.4 ± 0.1	9.0 ± 0.1	5.9 ± 0.1	0.4 ± 0.1	78.5 ± 1.1	15.3 ± 0.3

*Standard deviation; **not detected.

On the other hand, excessive hemicelluloses removal can hinder the obtainment of MFC/CNF gels. Dias et al. (2019) and Albornoz-Palma et al. (2020) explained that hemicelluloses, especially xylans, contribute to gel formation with fewer passes through the grinder. Because they are amorphous molecules, xylans can reduce the water output from fibers and potentiate the establishment of hydrogen bonds between cellulose and water, increasing the suspension viscosity during mechanical fibrillation (Afsahi et al. 2018, Claro et al. 2019). Moreover, it can be said that pre-treatments with Na_2SiO_3 were able to reduce the hemicellulose contents, but not harm the gel obtainment.

Dimension, homogeneity of particles, and turbidity

In the particles classes with an area smaller than 5 μm^2 (Figure 1), the frequencies obtained for *EUC SS 5 %* and *EUC SS 10 %* (~42 %) were slightly lower than those observed for *EUC control* (~45 %). Regarding this class, the highest frequency among treatments was observed for *PIN SS 10 %* (~56 %) followed by *PIN control* (~48 %) and *PIN SS 5 %* (~46 %).

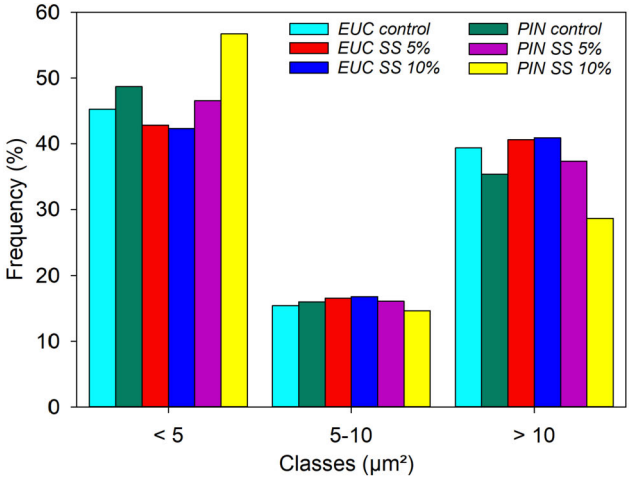

Figure 1: Classes of particles area of MFC/CNF suspensions from untreated and pre-treated pulps with sodium silicate solution in concentrations 5 % and 10 %.

For classes with areas between 5 and 10 μm^2, the frequencies were strongly similar among the pre-treatments studied. Regarding the particles class with areas larger than 10 μm^2, it was observed that *EUC SS 5 %* and *EUC SS 10 %* showed similar frequencies (~40 %) which were higher in relation to *EUC control* (~35 %). Also in this class, *PIN SS 5 %* (~37 %) presented higher frequencies than *PIN control* (~35) and *PIN SS 10 %* (~28 %).

For some pre-treatments, the particle area was slightly larger in relation to their respective controls. This indicates that the action of Na_2SiO_3 contributed to the greater efficiency of mechanical fibrillation. Furthermore, it is notable that *EUC control* and *PIN control* particles are composed of fibrils bundles of partially dissociated and cell wall fragments (arrows in Figure 2A).

Differently than indicated for controls, the particles with larger dimensions observed for *EUC SS 5 %* and *EUC SS 10 %* suspensions were formed by the aggregation of fibrils already individualized, much smaller, and thin cell wall fragments (arrows in Figures 2B and 2C). These characteristics were also observed for PIN MFC/CNF (arrows in Figures 2D, 2E, and 2F). Table 3 shows the averages for particle size as a function of the respective area class. Considering only the pre-treated pulps, around 59 and 71 % of the particles showed areas smaller than 10 μm^2 and with low standard deviation (< 3.4 μm^2), indicating greater homogeneity of the MFC/CNF suspension (Desmaisons et al. 2017).

Particle sizes affect the properties of MFC/CNF suspensions. Guimarães et al. (2016) and Turpeinen et al. (2020) explained that the viscosity and stability of MFC/CNF suspensions can be increased with a higher aspect ratio and homogeneity of particles. Therefore, it can be said that treatments with Na_2SiO_3 favored the obtainment of suspensions composed of particles with small diameters, greater lengths, and greater homogeneity. This can result in gel formation with fewer passes through the grinder and reduce energy consumption during the fibrillation process (Ang et al. 2019, Jaiswal et al. 2021). This effect is due to the alkaline action of Na_2SiO_3 solutions, which promotes the loosening of the cell walls of the fibers due to the removal of hemicelluloses and saponification of the intermolecular ester bonds, which increase the swelling capacity of the fibers and the surface area (Kamel et al. 2020, Noremylia et al. 2022), this potentiates the dissociation of fibril bundles from the abrasion of the grinder stones.

These results are consistent with other research. Mohtaschemi et al. (2014), when carrying out the mechanical fibrillation of Birch kraft pulp subjected to TEMPO-mediated oxidation, found CNF suspensions with thinner and more homogeneous structures. However, the authors detected the presence of fibers and particle fragments with dimensions in millimeter scales that entangled and formed aggregates, reducing the surface area of the MFC/CNF network. Žepič et al. (2014) and Osong et al.

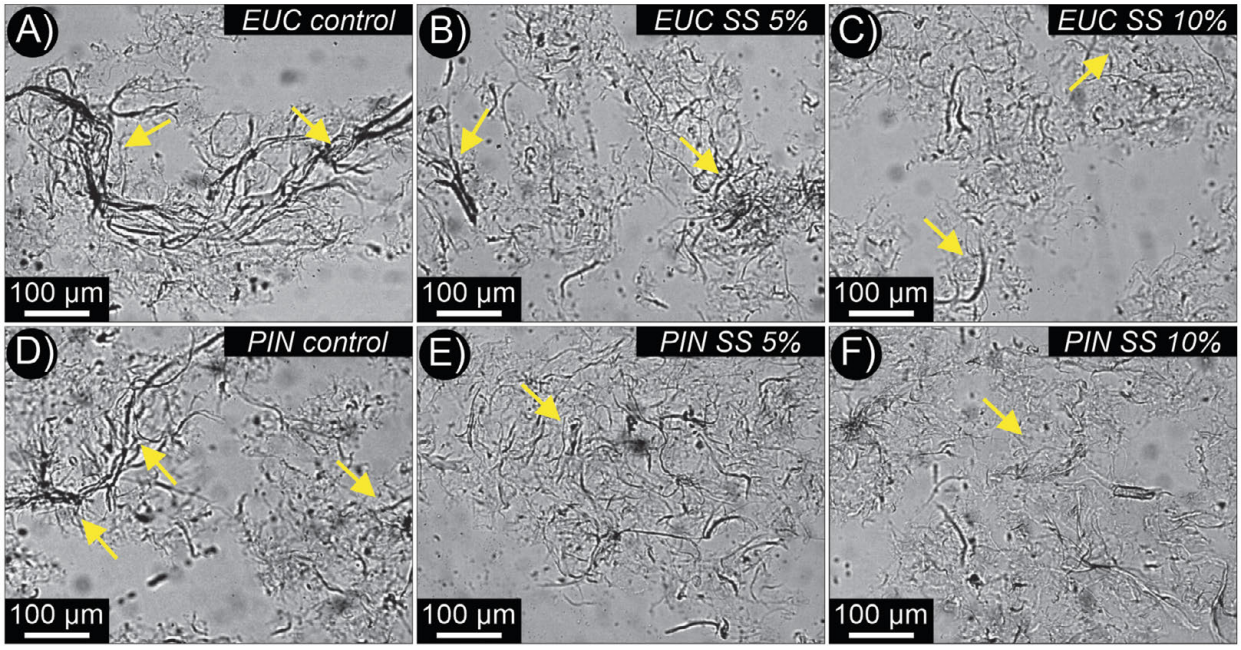

Figure 2: Images of light microscopy of MFC/CNF suspensions from untreated and pre-treated pulps with sodium silicate solution in concentrations 5 % and 10 % (10x magnification).

Table 3: Average and standard deviation of particles area of micro/nanofibril (MFC/CNF) suspensions from Eucalyptus sp. and Pinus sp., untreated and pre-treated with sodium silicate solutions in concentrations 5 % and 10 %.

Class (µm²)	Particles area (µm²)					
	EUC control	*EUC SS 5 %*	*EUC SS 10 %*	*PIN control*	*PIN SS 5 %*	*PIN SS 10 %*
< 5	2.3 ± 0.3*	2.4 ± 0.3	2.4 ± 0.3	2.3 ± 0.4	2.3 ± 0.3	2.3 ± 0.3
5-10	7.1 ± 1.2	7.1 ± 1.2	7.1 ± 1.2	7.1 ± 1.2	7.1 ± 1.2	7.0 ± 3.4
> 10	50.9 ± 160.2	47.4 ± 126.6	52.2 ± 139.6	44.9 ± 116.1	52.1 ± 164.9	46.9 ± 133.7
Average	20.1 ± 26.8	19.0 ± 24.7	20.6 ± 27.5	18.1 ± 23.3	20.5 ± 27.5	18.7 ± 24.5

*Standard deviation.

(2016) explained that in MFC/CNF suspensions there are nanofibrils, fibers, fine fibrils, fiber fragments, and fibril bundles, as presented in the present work. As a result, enzymatic or chemical pre-treatments are applied to the fibers before the mechanical fibrillation to facilitate the production of more homogeneous MFC/CNF suspensions, mainly containing nanoscale fragments (Santucci et al. 2016). Based on these aspects and the experimental results of this research, it can be said that this objective was achieved.

Turbidity results reinforce the reasoning presented since all the pre-treatments applied reduced the turbidity values compared to the controls. The lowest turbidity value of EUC MFC/CNF was observed for *EUC SS 10 %* pre-treatment. For PIN MFC/CNF, the lowest turbidity was obtained for *PIN SS 5 %* (Figure 3).

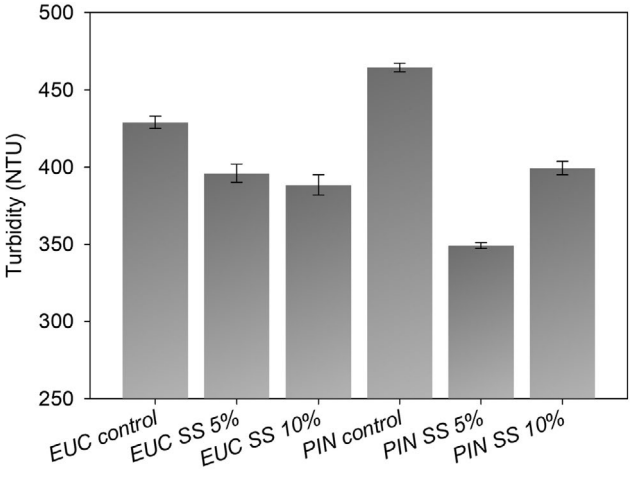

Figure 3: Turbity of MFC/CNF suspensions from untreated and pre-treated pulps with sodium silicate solution in concentrations 5 % and 10 %.

According to Bejoy et al. (2018), the purpose of this test is to measure the scattered light at an incidence angle of 90 °, the variation of the readings is related to the shape and refractive index of the dispersed material. The unit NTU from turbidimeter refers to nephelometric turbidity units. If the suspension is composed only of nanoscale particles, the turbidity value is close to zero. On the other hand, the presence of partially deconstructed fibers in the suspension will increase turbidity, as observed in the present work. The experimental results obtained for turbidity were in harmony with values found in other works. Qu et al. (2019) obtained turbidities ranging between 100 NTU and 500 NTU for CNF produced by mechanical fibrillation of kraft pulp from coniferous wood, after TEMPO-mediated oxidation. Moser et al. (2015) found turbidity values around 300 NTU when studying CNF obtained from coniferous pulp produced by fiber steam explosion.

Amini et al. (2020) evaluated the effect of different fine content on the turbidity of CNF suspensions and obtained values ranging between 400 NTU and 500 NTU. These authors observed that for higher fines content in the suspension, the turbidity values increased. These observations corroborate the understanding of the turbidity variation observed in the present study. As shown in Figure 2, different fibrillation conditions favored the different amounts of fines and aggregates in the suspensions.

Microstructure and physical properties of the films

The films obtained were visually homogeneous and malleable, being easily detached from the acrylic plates. Scanning electron microscopy showed a reduction in surface granularity of films with the application of Na_2SiO_3 (Figure 4).

Cell wall aggregates and fragments were observed on the *EUC control* and *PIN control* film surface, indicated by the arrows in Figures 4A and 4J, respectively. *EUC SS 5 %* and *EUC SS 10 %* films (Figures 4D and 4G) showed higher surface granularity in relation to *PIN SS 5 %* and *PIN SS 10 %* films (Figures 4M and 4P). In cross-sections, *EUC control* (Figures 4B and 4C) and *PIN control* (Figures 4K and 4L) films presented heterogeneous and discontinuous layers, due to the presence of cell wall fragments with different dimensions.

EUC SS 5 % (Figures 4E and 4F) and *EUC SS 10 %* (Figures 4H and 4I) films presented more cohesive and continuous layers in relation to the control. Similar characteristics were observed for *PIN SS 5 %* films (Figures 4N and 4O), in which the layers were vertically and horizontally more homogeneous. For *PIN SS 10 %* (Figures 4Q and 4R), there was a gap reduction between the MFC/CNF layers.

Greater granularities and roughness resulted in greater dispersion of incident light on the surface of the film, with a decrease in transparency (From et al. 2020). Films with a more granular surface show a greater contact surface, directly influencing the wettability (Aulin et al. 2009). This characteristic favors greater amounts of hydrogen bonds with water molecules. For this reason, adhesion forces overcome the cohesion forces, increasing the scattering of liquid on the film surface (Dimic-Misic et al. 2019). The thickness ranged between 20 µm and 36 µm (Figure 5A). The average thickness for *EUC control* was 18 % lower than *EUC SS 5 %* and 6 % greater than *EUC SS 10 %*. The smallest variation was observed for *EUC SS 5 %* films and the largest for *EUC SS 10 %*. Film thicknesses of *PIN SS 5 %* and *PIN SS 10 %* were 23 % and 12 % superior compared to *PIN control*, respectively.

Thickness is strongly influenced by the characteristics of the raw material and the concentration of MFC/CNF suspensions (Kolakovic et al. 2012). In the present study, the films were produced with identical suspension volume and solids content, which indicates that thickness variations observed were due to the effects of pre-treatments with Na_2SiO_3 in the film-forming suspensions. Kim et al. (2021) explained that MFC/CNF suspensions with lower gel formation, lower viscosity, and lower surface area, tend to form thinner films. This effect was observed in the present work because *EUC control* and *PIN control* films obtained the lowest average thickness. These materials presented suspensions with lower particle homogeneity, which indicates lower gel formation and lower surface area due to the larger aggregates of MFC/CNF (see Figure 2). All the films showed increments in grammage compared to the control (Figure 5B), except *PIN SS 10 %*. The grammages of *PIN SS 5 %* and *EUC SS 10 %* were similar (~31 g/m^2), while the highest average was obtained for *EUC SS 5 %* (~38 g/m^2). The lowest grammage averages were obtained for *PIN control*, *PIN SS 10 %*, and *EUC control*, respectively.

For bulk density, *EUC SS 5 %* and *EUC SS 10 %* presented averages, respectively, 8.6 % and 13.6 % higher in relation to *EUC control* (1007 kg/m^3) (Figure 5C). *PIN control*, *PIN SS 5 %*, and *PIN SS 10 %* showed the greatest variations in bulk density. Variation of the porosity of the film followed an inversely proportional trend in relation to bulk density (Figure 5D), as they are collinear parameters. Porosity varied between 20 % and 44 %, with the highest average observed for *PIN SS 10 %* and the lowest for *EUC SS 10 %*. Since the porosity variation was small, due to

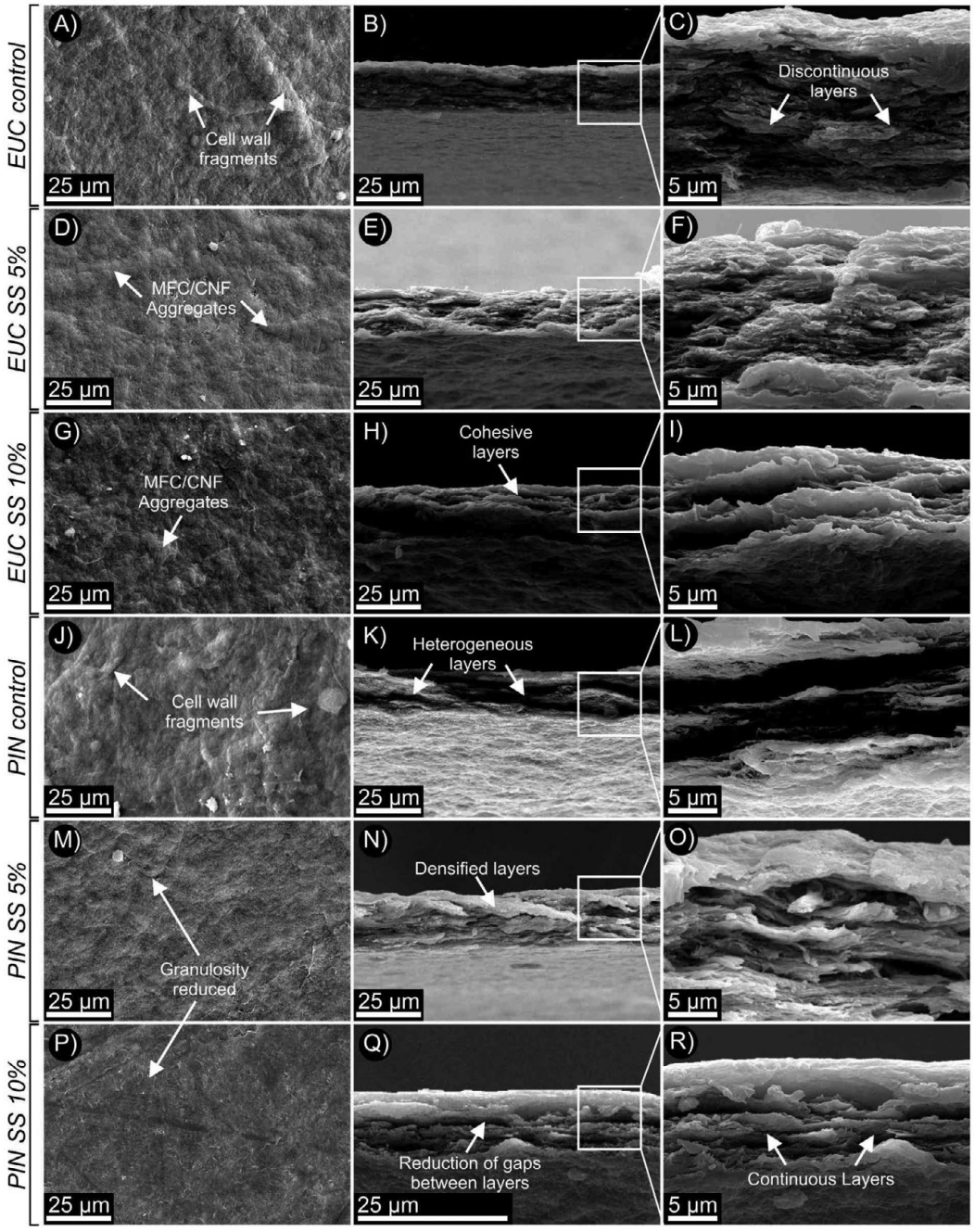

Figure 4: Micrographs of films of MFC/CNF from untreated and pre-treated pulps with sodium silicate solution in concentrations 5 % and 10 %; A) *EUC control* – surface; B) *EUC control* – cross section and C) *EUC control* – cross section zoom; D) *EUC SS 5 %* – surface; E) *EUC SS 5 %* – cross section; F) *EUC SS 5 %* – cross section zoom; G) *EUC SS 10 %* – surface; H) *EUC SS 10 %* – cross section; I) *EUC SS 10 %* – cross section zoom; J) *PIN control* – surface; K) *PIN control* – cross section; L) *PIN control* – cross section zoom; M) *PIN SS 5 %* – surface; N) *PIN SS 5 %* – cross section; O) *PIN SS 5 %* – cross section zoom; P) *PIN SS 10 %* – surface; Q) *PIN SS 10 %* – cross section; and R) *PIN SS 10 %* – cross section zoom.

low standard deviation, the results indicated that the films produced were relatively homogeneous. For suspensions with larger particle sizes, and in which the "gel point" was probably prolonged (EUC *control* and PIN *control*), porosity averages were slightly higher.

Raj et al. (2015) reported that reduced "gel point" results in increased porosity of CNF composites, suggesting that the three-dimensional open/porous structure of cellulose suspension is partially maintained during the formation of the two-dimensional film structure. Research re-

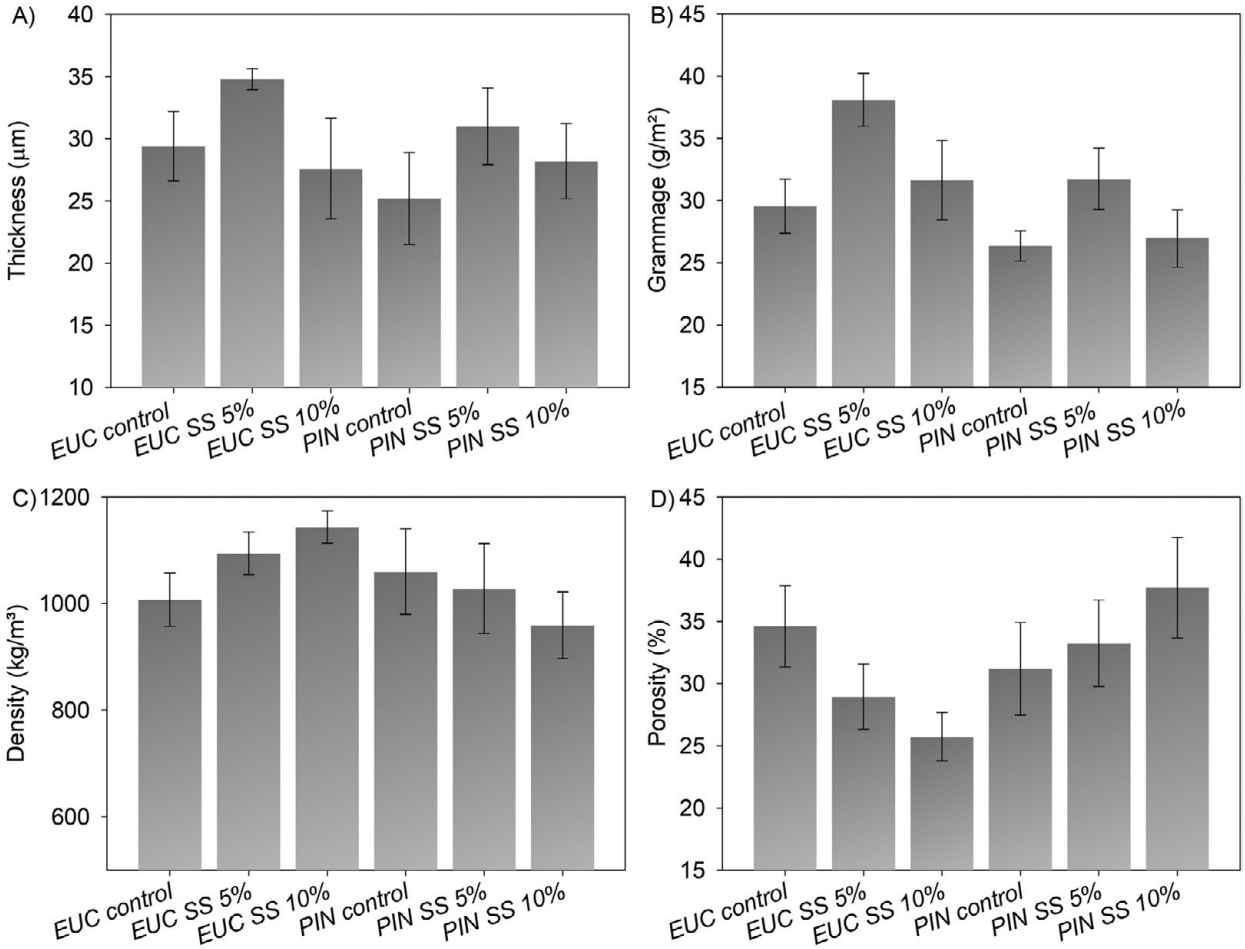

Figure 5: A) Thickness; B) grammage; C) bulk density; and D) porosity of films of MFC/CNF suspensions from untreated and pre-treated pulps with sodium silicate solutions in concentrations 5 % and 10 %.

ports that thickness, density, and porosity are determining parameters of the characteristics of the film, as they are strongly related to mechanical, optical, and barrier properties to water vapor and gases (Fukuzumi et al. 2013, Bedane et al. 2015). Additionally, part of the variations observed for the parameters studied can be explained by the characteristics inherent to the *casting* method, which is widely used in research with cellulose, starch, and protein-based films (Suhag et al. 2020). Production of films with larger dimensions is limited, the time of solvent evaporation is prolonged and the films may present heterogeneity in thickness and wrinkling because the method does not apply vacuum (Moraes et al. 2013, Espitia et al. 2014). Even so, the results found are in harmony with other works from the literature. Cruz et al. (2022) found average thicknesses for MFC/CNF films of EUC and PIN around 35 and 32 µm, respectively. For MFC/CNF films of PIN, Mascarenhas et al. (2022) found a thickness value close to 21 µm and bulk density of 1050 kg/m^3.

Light transmittance and transparency of the films

The films showed different transmittance intensities across the entire wavelength range, indicating the influence of Na_2SiO_3 pre-treatments (Figure 6A). Most films showed transmittance below 15 % and only *PIN SS 5 %* and *PIN SS 10 %* showed transmittance below 10 %. For cellulose films, transmittance values in this range indicate suitable UV light barrier properties (Cazón et al. 2020). This characteristic is interesting for applications in the packaging of products susceptible to degradation by UV light, such as some foods and medicines (Niu et al. 2018, Bastante et al. 2021). For UVB wavelength from 280 to 315 nm, the highest transmittance was observed for *EUC control* film followed by *PIN control*, *EUC SS 5 %*, *EUC SS 10 %*, *PIN SS 10 %*, and *PIN SS 5 %*. The same order was observed for transmittance in the UVA range (315-400 nm). For both

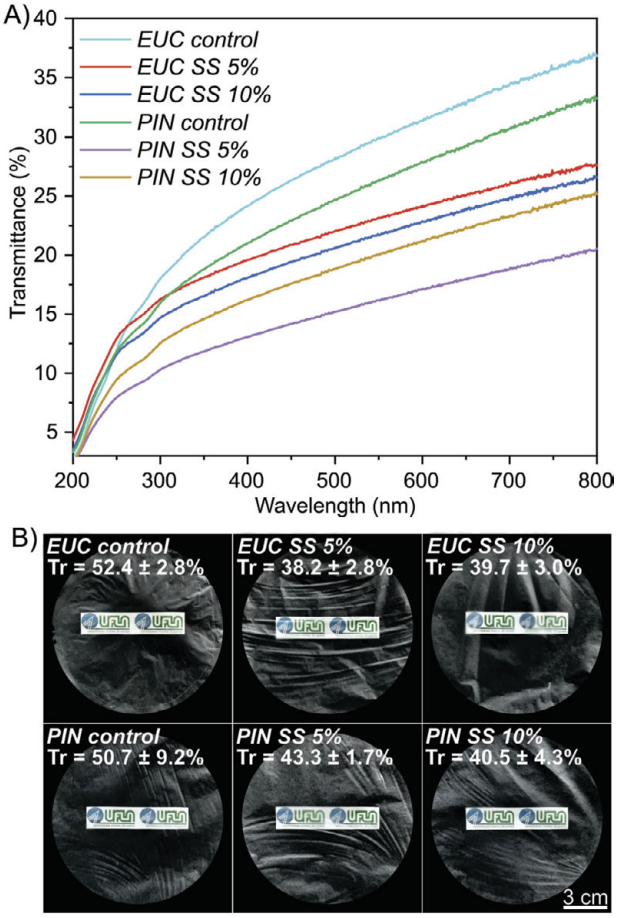

Figure 6: A) Transmittance; and B) transparency (Tr) of films of MFC/CNF suspensions from untreated and pre-treated pulps with sodium silicate solution in concentrations 5 % and 10 %.

UVB and UVA, transmittance rates were low, confirming that the films produced are translucent (Kim et al. 2021).

For the visible light region (400–700 nm), the transmittance for *EUC control* and *PIN control* ranged between 21 % and 34 %. For *EUC SS 5 %*, *EUC SS 10 %*, and *PIN SS 10 %*, the transmittance range was between 16 % and 26 %, whereas for *PIN SS 5 %*, the transmittance ranged from 12 % to 19 %. The infrared region (> 700 nm), confirmed the same trends described for the visible light region, with increased transmittance intensity with Na_2SiO_3 pre-treatment.

Transmittance values for *EUC SS 5 %* and *EUC SS 10 %* were 27 % and 24 % higher than the *EUC control*, respectively. Compared to the *PIN control*, the transmittances for *PIN SS 5 %* and *PIN SS 10 %* were 15 % and 20 % higher, respectively. In general, variations for Tr between treatments were low. Considering only MFC/CNF films from pre-treatments, the Tr values obtained for PIN were slightly higher than those found for EUC.

The transparency of MFC/CNF films can be influenced by the dimensions of cellulose fibrils, fiber aggregates, degree of homogenization, and the granularity/roughness of the film surface (Mascarenhas et al. 2022). The granularity was lower for *PIN SS 5 %* and *PIN SS 10 %* (see Figures 4M and 4P). MFC/CNF diameters are smaller in relation to the wavelength of visible light, as a result, dense packing of cellulose bundles can cause suppression or projection of light scattering, depending on the fibrillation degree (Kumar et al. 2014).

The transparency is also affected by the MFC/CNF crystal structure, therefore, as smaller the dimensions of the crystallites present in the cellulose aggregates, the greater the light scattering, which results in lower transparency (Zhang et al. 2015). The results indicated improvements in the optical properties, mainly regarding the barrier to UVC. This aspect is important for the application of the film, as transparency is configured as an important indicator for the commercial destination, such as packaging (Jing et al. 2022). The highest opacity values were obtained for EUC control (~59 %) and *PIN SS 5 %* (~60 %) while the lowest value was found for *EUC SS 5 %* (~53 %) (Figure 7). Films produced with *EUC SS 10 %*, PIN control, and *PIN SS 10 %* showed intermediate opacity values (~55 %).

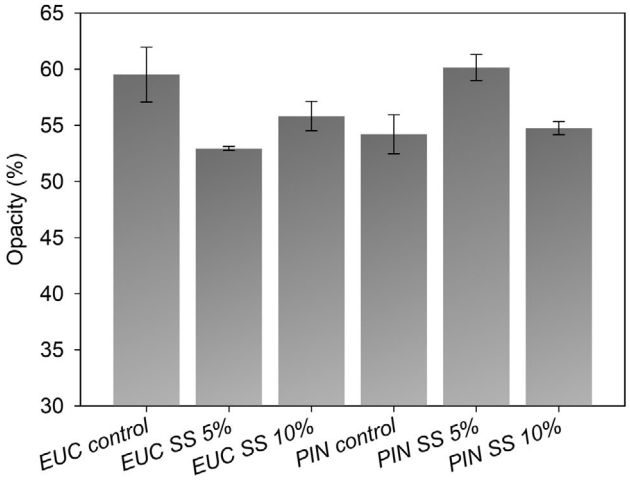

Figure 7: Opacity of films of MFC/CNF suspensions from untreated and pre-treated pulps with sodium silicate solution in concentrations 5 % and 10 %.

The higher opacity can be explained by the presence of cell wall particles, bundles of fibrils, and MFC/NFC aggregates in the composition of the films, as seen in Figure 4. Larger fragments offer a greater barrier to the passage of light through the films (Wang et al. 2013), as evidenced by the transmittance results.

The opacity in some cases can more consistently explain aspects related to the influence of the degree of fibrillation and the dimensions of the MFC/NFC in the films. Hsieh et al. (2017) and Xinping et al. (2020) explained that the presence of larger fragments in NFC films/nanopapers from bleached materials may allow the passage of light because they have certain transparency. This may contribute to the overestimation of transparency values, which will not necessarily be associated with a higher degree of fibrillation and may represent higher opacity values (Yang et al. 2019a, Hou et al. 2020).

Barrier properties and grease resistance

The highest values of WVTR were observed for *EUC control* and *PIN SS 10 %*, whereas the other films presented values ranging from 1170 to 1220 g/m^2 day (Figure 8A). The WVP averages of the films were decreased in the following order: *EUC SS 5 %*, *EUC SS 10 %*, *PIN SS 5 %*, *EUC control*, *PIN SS 10 %*, and *PIN control* (Figure 8B).

For *EUC SS 5 %* the WVP was slightly higher because the films were thicker in relation to other treatments. As already mentioned, it is possible that excessive fibrillation affected the three-dimensional structure of the MFC/CNF network, reducing the number of interfibrillar interactions and allowing the formation of isolated aggregates. This results in the appearance of regions with void spaces in the films, facilitating the passage of water vapor (Li et al. 2019).

Based on the TAPPI T 559 cm-12 standard (TAPPI 2012), all the films were resistant to kit 12, which is more aggressive because it contains higher n-heptane and toluene amounts. This indicates that the films present a high barrier to the fats penetration and the ability to retain fine and viscous oils, which can be found in foods, grains, and waxes. This result is in accordance with other research, which reports that films and paper coatings based on MFC/CNF present resistance to oil penetration (Tyagi et al. 2018, Jin et al. 2021).

Cruz et al. (2022) and Mascarenhas et al. (2022) also observed high resistance to oil penetration in MFC/CNF films from *Eucalyptus* sp. and *Pinus* sp. The authors explained that because the MFC/CNF diameters are very small, the layers architecture of the films tends to be strongly closed and difficult for being penetrated by viscous liquid.

According to the classification presented by Wang et al. (2018), it can be considered that all films presented an average barrier to water vapor because the WVP values were between 0.4 g mm/day m^2 kPa and 4 mm/day m^2 kPa. These authors also reported that films with these characteristics could be used for food packaging, depending on their nature. The films evaluated in the present study meet the WVTR and thickness for package bakery products, fruits, and salads (Wang et al. 2018).

WVP values obtained in the present work were lower than results found in the literature, demonstrating that the pre-treatments performed contributed to the barrier properties improvement. This is an advantage because in general, MFC/CNF are combined with synthetic polymers, proteins, and minerals to improve gas barrier properties (Zhang et al. 2021).

Hasan et al. (2021) found WVP values ranging from 5 mm/day m^2 kPa to 25 mm/day m^2 kPa when analyzing different techniques for film production obtained

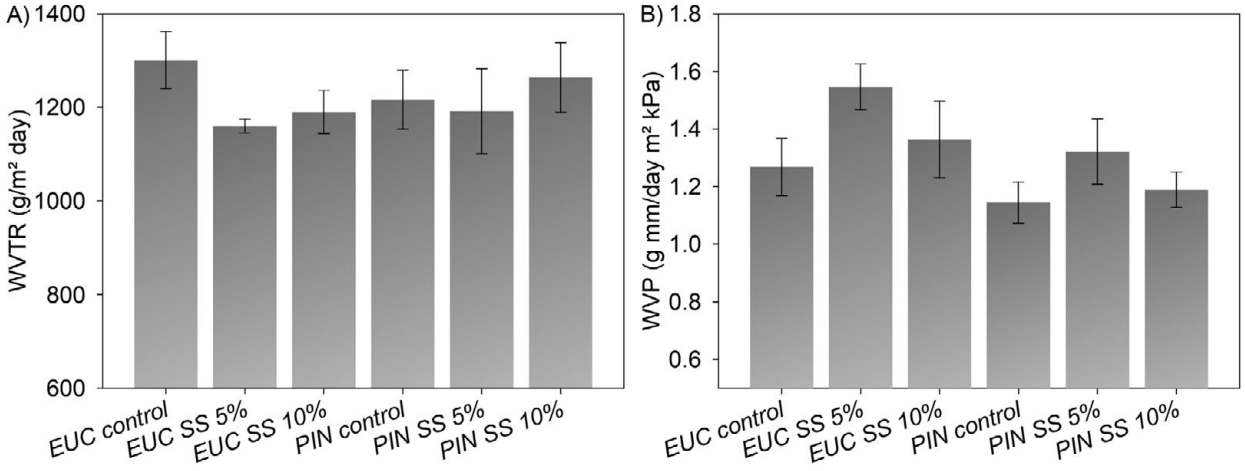

Figure 8: A) Water vapor transmission rate (WVTR) and B) water vapor permeability (WVP) of films of MFC/CNF suspensions from untreated and pre-treated pulps with sodium silicate solution in concentrations 5 % and 10 %.

from CNF from untreated coniferous fibers by mechanical fibrillation. Wang et al. (2020) found WVP around 5.5 mm/day m^2 kPa and 12 mm/day m^2 kPa for NFC films. Nascimento et al. (2021), studying films composed of cellulose nanocrystals and bacterial nanocellulose, found WVP values ranging from 2.96 mm/day m^2 kPa and 3.57 mm/day m^2 kPa. Evaluation of permeability is important in choosing a better destination for the films. For applications involving foods like fresh vegetables, permeable films could be applied, while poorly permeable films can be indicated for foods and dehydrated products (Lago et al. 2020).

Mechanical properties of the films

EUC SS 10 % achieved tensile strength of ~82 MPa, 17 % higher compared to *EUC control* (Figure 9A). The strength of *PIN SS 10 %* (~70 MPa) was around 20 % higher in relation to *PIN control*. The highest values for Young's modulus (Figure 9B) were found for *EUC SS 5 %* (~4 GPa) and *PIN SS 10 %* (~3.5 GPa), while the lowest value was obtained for *PIN control* (~1.7 GPa). These results indicate that the pretreatments proposed promoted improvements in mechanical properties, especially for *EUC SS 10 %*.

Films with higher density showed higher values of tensile strength. Yang et al. (2019b) and Liang et al. (2020) explained that MFC/CNF present absolutely small dimensions, which favors the obtainment films with high layer compaction and a great number of hydrogen bonds. As a result, there is an increase in density and greater slipping resistance in the structure of the film, when subjected to tensile stress. Analyzing the results of Young's modulus and elongation at break (Figure 9C), it is possible to note that films with lower strength presented lower elongation (< 8 %), lower energy absorption, and presented lower tenacity when compared to films with higher strength (*EUC SS 5 %* and *EUC SS 10 %*). Verker et al. (2009) ex-

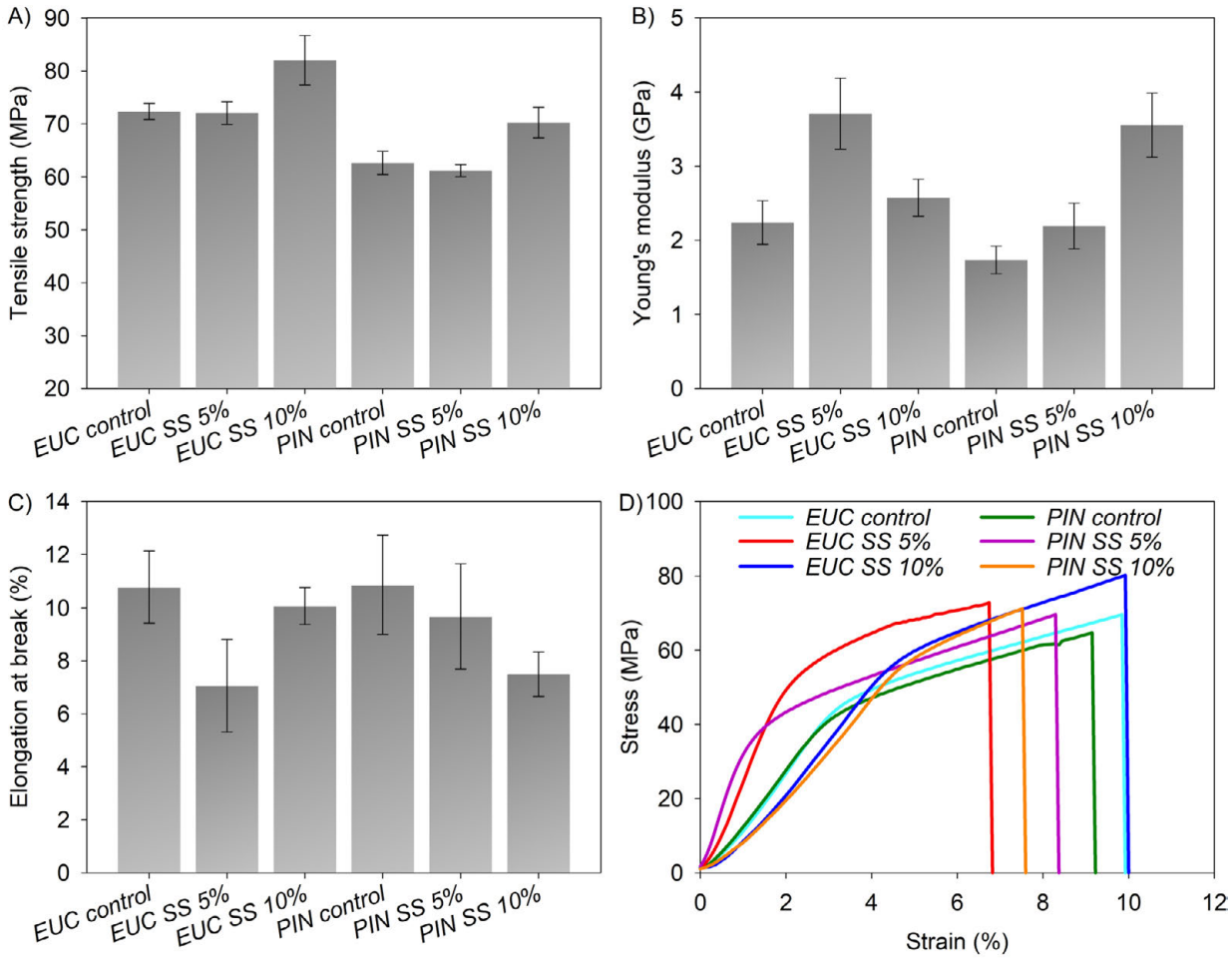

Figure 9: A) Tensile strength; B) Young's modulus; C) elongation at break; and D) stress x strain curves (tensile test) of films of MFC/CNF suspensions from untreated and pre-treated pulps with sodium silicate solution in concentrations 5 % and 10 %.

plained that films with this characteristic release the highest percentage of energy absorbed in the elastic phase, as observed for *EUC control*, *PIN control*, and *EUC SS 10 %* (Figure 9D).

In general, films presented strengths consistent with other studies. Noorbakhsh-Soltani et al. (2018) when studying nanocellulose and chitosan films for food packaging, found tensile strength ranging between 60 and 70 MPa and Young's modulus between 2 and 4 GPa. Wang et al. (2020) evaluated films produced with different proportions of CNC/CNF for application in packaging and obtained tensile strength around 40–80 MPa and Young's modulus ranging from 2 to 7 GPa.

Quality index of the cellulose micro/nanofibrils

The QI values for MFC/CNF of EUC and PIN were similar, ranging between ~53 and ~58. However, for *EUC SS 10 %* (~70), the IQ values were 16 % higher in relation to other treatments (Figure 10).

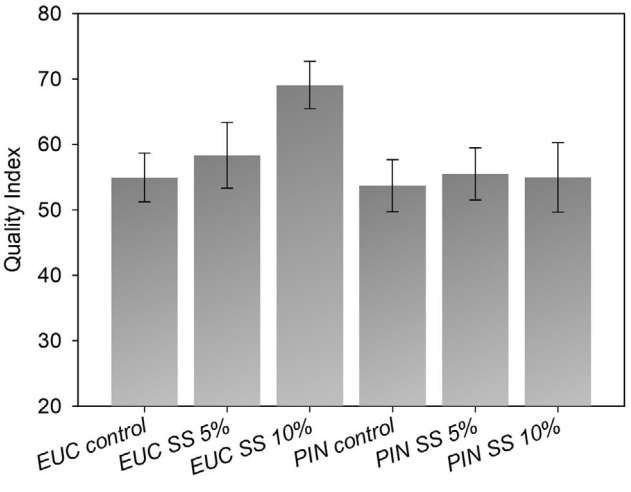

Figure 10: Quality Index (QI) of MFC/CNF suspensions from untreated and pre-treated pulps with sodium silicate solution in concentrations 5 % and 10 %.

Research indicates that QI is related to energy consumption during mechanical fibrillation. Desmaisons et al. (2017) reported that QI values between 50–70 are characteristic of MFC/CNF produced with energy consumption of around 5000 kWh/t. Banvillet et al. (2021a) found QI values ranging between 40–60 when producing CNF from pulps treated with 10 % NaOH (w/w). The authors found that these QI values are according to energy consumption between 2000–5000 kWh/t during mechanical fibrillation. In the present work, the energy consumption until the gel consistency was between 3000–4100 kWh/t for *EUC control* and 4400–4500 kWh/t for *PIN control*.

Besides correlating with energy consumption, QI is also calculated based on the suspension properties and resulting film/nanopaper, including particle dimensions in multiple length scales (Desmaisons et al. 2018). Comparing the results obtained in Rol et al. (2019), Banvillet et al. (2021a), and Dias et al. (2022) QI values from the present study were comparable to those obtained for pre-treatments already established and with potential for industrial application, such as pre-treatment with NaOH solution 10 % (QI between 54–82), oxidation with periodates – sulfonation, $NaBH_4$, amines, and ClO_2 (~62), carboxymethylation (~66), enzymatic pre-treatments (68–75) and pre-treated fibers with deep eutectic solvent (66–72).

Given the reduced number of studies addressing QI, the studies mentioned corroborate the results found in the present research, because the QI was in accordance with the same variation presented in the literature. Moreover, it can be said that Na_2SiO_3 proved to be efficient, improving the MCF/CNF individualization, being a low-cost alternative, and with effects similar to other successful pre-treatments.

Conclusion

Fibers from *Eucalyptus* sp. and *Pinus* sp. were treated with Na_2SiO_3 to reduce energy consumption in mechanical fibrillation, evaluating the properties of suspensions, films, and posteriorly, calculating QI. Pre-treatments with Na_2SiO_3 resulted in greater individualization, greater homogeneity, and lower turbidity of the MFC/CNF suspensions. Films properties were strongly influenced by the suspension characteristics. The transparency of the films produced with treated fiber was ~22 % lower compared to the controls. Barrier properties to grease were suitable for all the treatments, although the same was not observed for the barrier to water vapor. Young's modulus was increased from 2 to 4 GPa for both pulps with the treatment with 10 % of Na_2SiO_3. Considering the greater individualization capacity of MFC/NFC, a greater barrier to UV radiation, less water vapor penetration, and greater tensile strength, the best results were found for MFC/NFC obtained from EUC and PIN pre-treated with 10 % Na_2SiO_3. As for the QI, the highest values were found for the PIN MFC/CNF obtained with pre-treatment with 10 % Na_2SiO_3

(~ 70). For EUC fibers, the highest QI values (~ 58) were found for MFC/NFC obtained from the pre-treatment using 5 % Na_2SiO_3. The suspensions showed interesting characteristics for applications in the form of emulsion stabilizers. The films presented microstructural, physical, optical, barrier, and mechanical properties suitable to the parameters required for packaging. The experimental results indicate that the use of Na_2SiO_3 as fibers pre-treatment for production of MFC/CNF has potential for industrial scaling up, with low cost and similar to other pre-treatments already established.

Acknowledgments: We are especially grateful to the Program in Wood Science and Technology (PPGCTM) of the Federal University of Lavras (UFLA) for providing study material and infrastructure. We would also like to thank Embrapa Instrumentação and Klabin S. A. for the availability of inputs and equipment for the analysis required in this work. The authors are also grateful to the Coordination for the Improvement of Superior Education Personnel (CAPES) and Amapá Research Support Foundation (FAPEAP) for providing the research grant.

Funding: The research was funded by the National Council for Scientific and Technological Development (CNPq) (finance code 300985/2022-3).

Conflict of interest: The authors declare that there are no conflicts of interest.

References

Afsahi, G., Dimic-Misic, K., Gane, P., Budtova, T., Maloney, T., Vuorinen, T. (2018) The investigation of rheological and strength properties of NFC hydrogels and aerogels from hardwood pulp by short catalytic bleaching (Hcat). Cellulose 25:1637–1655. https://doi.org/10.1007/s10570-018-1678-6.

Albornoz-Palma, G., Ching, D., Valerio, O., Mendonça, R.T., Pereira, M. (2020) Effect of lignin and hemicellulose on the properties of lignocellulose nanofibril suspensions. Cellulose 27:10631–10647. https://doi.org/10.1007/s10570-020-03304-5.

Amalraj, A., Gopi, S., Thomas, S., Haponiuk, J.T. (2018) Cellulose nanomaterials in biomedical, food, and Nutraceutical Applications: A Review. Macromol. Symp. 380:1800115. https://doi.org/10.1002/masy.201800115.

Amini, E., Hafez, I., Tajvidi, M., Bousfield, D.W. (2020) Cellulose and lignocellulose nanofibril suspensions and films: A comparison. Carbohydr. Polym. 250:117011. https://doi.org/10.1016/j.carbpol.2020.117011.

Ang, S., Haritos, V., Batchelor, W. (2019) Effect of refining and homogenization on nanocellulose fiber development, sheet strength and energy consumption. Cellulose 26:4767–4786. https://doi.org/10.1007/s10570-019-02400-5.

ASTM Standard (2012) E-104-02, Standard Practice for Maintaining Constant Relative Humidity by Means of Aqueous Solutions.

ASTM Standard (2016) ASTM E-96, Standard Test Methods for Water Vapor Transmission of Materials.

ASTM Standard (2018) ASTM D882-18, Standard Test Methods for Tensile Properties of Thin Plastic Sheeting.

Aulin, C., Yun, S.H., Wagberg, L., Lindström, T. (2009) Design of Highly Oleophobic Cellulose Surfaces from Structured Silicon Templates. Appl. Mater. Interfaces 1:2443–2452. https://doi.org/10.1021/am900394y.

Balea, A., Fuente, E., Monte, M.C., Merayo, N., Campano, C., Negro, C., Blanco, A. (2020) Industrial Application of Nanocelluloses in Papermaking: A Review of Challenges, Technical Solutions, and Market Perspectives. Molecules 25:256. http://dx.doi.org/10.3390/molecules25030526.

Banvillet, G., Depres, G., Belgacem, N., Bras, J. (2021a) Alkaline treatment combined with enzymatic hydrolysis for efficient cellulose nanofibrils production. Carbohydr. Polym. 255:117383. https://doi.org/10.1016/j.carbpol.2020.117383.

Banvillet, G., Gatt, E., Belgacem, N., Bras, J. (2021b) Cellulose fibers deconstruction by twin-screw extrusion with in situ enzymatic hydrolysis via bioextrusion. Bioresour. Technol. 327:124819. https://doi.org/10.1016/j.biortech.2021.124819.

Bastante, C.C., Silva, N.H.C.S., Cardoso, L.C., Serrano, C.M., Ossa, E.J.M., Freire, C.S.R., Vilela, C. (2021) Biobased films of nanocellulose and mango leaf extract for active food packaging: Supercritical impregnation versus solvent casting. Food Hydrocoll. 117:106709. https://doi.org/10.1016/j.foodhyd.2021.106709.

Bedane, A.H., Eic, M., Farmahini-Farahani, M., Xiao, H. (2015) Water vapor transport properties of regenerated cellulose and nanofibrillated cellulose films. J. Membr. Sci. 493:46–57. https://doi.org/10.1016/j.memsci.2015.06.009.

Bejoy, T., Midhun, C.R., Athira, K.B., Rubiyah, M.H., Jithin, J., Audrey, M., Drisko, G.L., Sanchez, C. (2018) Nanocellulose, a Versatile Green Platform: From Biosources to Materials and Their Applications. Chem. Rev. 24:11575–11625. https://doi.org/10.1021/acs.chemrev.7b00627.

Berto, G.L., Arantes, V. (2019) Kinetic changes in cellulose properties during defibrillation into microfibrillated cellulose and cellulose nanofibrils by ultra-refining. Int. J. Biol. Macromol. 127:637–648. https://doi.org/10.1016/j.ijbiomac.2019.01.169.

Cazón, P., Velazquez, G., Vázquez, M. (2020) Characterization of mechanical and barrier properties of bacterial cellulose, glycerol and polyvinyl alcohol (PVOH) composite films with eco-friendly UV-protective properties. Food Hydrocolloides 99:105323. https://doi.org/10.1016/j.foodhyd.2019.105323.

Chanda, S., Bajwa, D.S. (2021) A review of current physical techniques for dispersion of cellulose nanomaterials in polymer matrices. Rev. Adv. Mater. Sci. 60:325–341. https://doi.org/10.1515/rams-2021-0023.

Claro, F.C., Matos, M., Jordão, C., Avelino, F., Lomonaco, D., Magalhães, W.L.E. (2019) Enhanced microfibrillated cellulose-based film by controlling the hemicellulose content and MFC rheology. Carbohydr. Polym. 218:307–314. https://doi.org/10.1016/j.carbpol.2019.04.089.

Cruz, T.M., Mascarenhas, A.R.P., Scatolino, M.V., Faria, D.L., Matos,

L.C., Duarte, P.J., Neto, J.M., Mendes, L.M., Tonoli, G.H.D. (2022) Hybrid films from plant and bacterial nanocellulose: mechanical and barrier properties. Nord. Pulp Pap. Res. J. 37(1). https://doi.org/10.1515/npprj-2021-0036.

Desmaisons, J., Boutonnet, E., Rueff, M., Dufresne, A., Bras, J. (2017) A new quality index for benchmarking of different cellulose nanofibrils. Carbohydr. Polym. 174:318–329. https://doi.org/10.1016/j.carbpol.2017.06.032.

Desmaisons, J., Gustafsson, E., Dufresne, A., Bras, J. (2018) Hybrid nanopaper of cellulose nanofibrils and PET microfibers with high tear and crumpling resistance. Cellulose 25:7127–7142. https://doi.org/10.1007/s10570-018-2044-4.

Dias, M.C., Belgacem, M.N., Resende, J.V., Martins, M.A., Damásio, R.A.P., Tonoli, G.H.D., Ferreira, S.R. (2022) Eco-friendly laccase and cellulase enzymes pretreatment for optimized production of high content lignin-cellulose nanofibrils. Int. J. Biol. Macromol. 209:413–425. https://doi.org/10.1016/j.ijbiomac.2022.04.005.

Dias, M.C., Mendonça, M.C., Damásio, R.A.P., Zidanes, U.L., Mori, F.A., Ferreira, S.R., Tonoli, G.H.D. (2019) Influence of hemicellulose content of *Eucalyptus* and *Pinus* fibers on the grinding process for obtaining cellulose micro/nanofibrils. Holzforschung 73:1035–1046. https://doi.org/10.1515/hf-2018-0230.

Dimic-Misic, K., Kostic, M., Obradovic, B., Kramar, A., Jovanovic, S., Stepanenko, D., Mitrovic-Dankulov, M., Lazovic, S., Johansson, L.S., Maloney, T., Gane, P. (2019) Nitrogen plasma surface treatment for improving polar ink adhesion on micro/nanofibrillated cellulose films. Cellulose 26:3845–3857. https://doi.org/10.1007/s10570-019-02269-4.

Espinosa, E., Rol, F., Bras, J., Rodríguez, A. (2020) Use of multi-factorial analysis to determine the quality of cellulose nanofibers: effect of nanofibrillation treatment and residual lignin content. Cellulose 27:10689–10705. https://doi.org/10.1007/s10570-020-03136-3.

Espitia, P.J.P., Du, W.X., Avena-Bustillos, R.J., Soares, N.F.F., Mchugh, T.H. (2014) Edible films from pectin: Physical-mechanical and antimicrobial properties - A review. Food Hydrocoll. 35:287–296. https://doi.org/10.1016/j.foodhyd.2013.06.005.

Fakhouri, F.M., Costa, D., Yamashita, F., Martelli, S.M., Jesus, R.C., Alganer, K., Collares-Queiroz, F.P., Innocentini-Mei, L.H. (2013) Comparative study of processing methods for starch/gelatin films. Carbohydr. Polym. 95:681–689. https://doi.org/10.1016/j.carbpol.2013.03.027.

Fonseca, A.S., Panthapulakkal, S., Konar, S.K., Sain, M., Bufalino, L., Raabe, J., Miranda, I.P.A., Martins, M.A., Tonoli, G.H.D. (2019) Improving cellulose nanofibrillation of non-wood fiber using alkaline and bleaching pre-treatments. Ind. Crop. Prod. 131:203–212. https://doi.org/10.1016/j.indcrop.2019.01.046.

From, M., Larsson, P.T., Andreasson, B., Medronho, B., Svanedal, I., Edlund, H., Norgren, M. (2020) Tuning the properties of regenerated cellulose: Effects of polarity and water solubility of the coagulation medium. Carbohydr. Polym. 236:116068. https://doi.org/10.1016/j.carbpol.2020.116068.

Fukuzumi, H., Saito, T., Isogai, A. (2013) Influence of TEMPO-oxidized cellulose nanofibril length on film properties. Carbohydr. Polym. 93:172–177. https://doi.org/10.1016/j.carbpol.2012.04.069.

Grigatti, M., Montecchio, D., Francioso, O., Ciavatta, C. (2015) Structural and Thermal Investigation of Three Agricultural Biomasses Following Mild-NaOH Pretreatment to Increase Anaerobic Biodegradability. Waste Biomass Valoriz. 6:1135–1148. https://doi.org/10.1007/s12649-015-9423-y.

Guan, Q.F., Yang, H.B., Han, Z.M., Zhou, L.C., Zhu, Y.B., Ling, Z.C., Jiang, H.B., Wang, P.F., Ma, T., Wu, H.A., Yu, S.H. (2020) Lightweight, tough, and sustainable cellulose nanofiber-derived bulk structural materials with low thermal expansion coefficient. Sci. Adv. 6:eaaz1114. https://doi.org/10.1126/sciadv.aaz1114.

Guimarães, I.C., Reis, K.C., Menezes, E.G.T., Rodrigues, A.C., Silva, T.F., Oliveira, I.R.N., Boas, E.V.B. (2016) Cellulose microfibrillated suspension of carrots obtained by mechanical defibrillation and their application in edible starch films. Ind. Crop. Prod. 89:285–294. https://doi.org/10.1016/j.indcrop.2016.05.024.

Hasan, I., Wang, J., Tajvidi, M. (2021) Tuning physical, mechanical and barrier properties of cellulose nanofibril films through film drying techniques coupled with thermal compression. Cellulose 28:11345–11366. https://doi.org/10.1007/s10570-021-04269-9.

Hashem, M., El-Bisi, M., Sharaf, S., Refaie, R. (2010) Pre-cationization of cotton fabrics: An effective alternative tool for activation of hydrogen peroxide bleaching process. Carbohydr. Polym. 79:533–540. https://doi.org/10.1016/j.carbpol.2009.08.038.

Hou, G., Liu, Y., Li, D.Z.G., Xie, H., Fang, Z. (2020) Approaching Theoretical Haze of Highly Transparent All-Cellulose Composite Films. ACS Appl. Mater. Interfaces 12:31998–32005. https://dx.doi.org/10.1021/acsami.0c08586.

Hsieh, M.C., Koga, H., Suganuma, K., Nogi, M. (2017) Hazy Transparent Cellulose Nanopaper. Sci. Rep. 7:41590. https://doi.org/10.1038/srep41590.

Jaiswal, A.K., Kumar, V., Khakalo, A., Lahtinen, P., Solin, K., Pere, J., Toivakka, M. (2021) Rheological behavior of high consistency enzymatically fibrillated cellulose suspensions. Cellulose 28:2087–2104. https://doi.org/10.1007/s10570-021-03688-y.

Jin, K., Tang, Y., Liu, J., Wang, J., Ye, C. (2021) Nanofibrillated cellulose as coating agent for food packaging paper. Int. J. Biol. Macromol. 168:331–338. https://doi.org/10.1016/j.ijbiomac.2020.12.066.

Jing, M., Zhang, L., Fan, Z., Liu, X., Wang, Y., Chuntai, L., Shen, C. (2022) Markedly improved hydrophobicity of cellulose film via a simple one-step aminosilane-assisted ball milling. Carbohydr. Polym. 275:119701. https://doi.org/10.1016/j.carbpol.2021.118701.

Kamel, R., El-Wakil, N.A., Dufresne, A., Elkasabgy, N.A. (2020) Nanocellulose: From an agricultural waste to a valuable pharmaceutical ingredient. Int. J. Biol. Macromol. 163:1579–1590. https://doi.org/10.1016/j.ijbiomac.2020.07.242.

Karina, M., Satoto, R., Abdullah, A.D., Yudianti, R. (2020) Properties of nanocellulose obtained from sugar palm (*Arenga pinnata*) fiber by acid hydrolysis in combination with high-pressure homogenization. Cellul. Chem. Technol. 54:33–38. http://dx.doi.org/10.35812/CelluloseChemTechnol.2020.54.04.

Kim, H.J., Roy, S., Rhim, J.W. (2021) Effects of various types of cellulose nanofibers on the physical properties of the CNF-based films. J. Environ. Chem. Eng. 9:106043. https://doi.org/10.1016/j.jece.2021.106043.

Kolakovic, R., Peltonen, L., Laukkanen, A., Hirvonen, J., Laaksonen,

T. (2012) Nanofibrillar cellulose films for controlled drug delivery. Eur. J. Pharm. Biopharm. 82:308–315. https://doi.org/10.1016/j.ejpb.2012.06.011.

Kumar, V., Bollström, R., Yang, A., Chen, Q., Chen, G., Salminen, P., Bousfield, D., Toivakka, M. (2014) Comparison of nano- and microfibrillated cellulose films. Cellulose 21:3443–3456. https://doi.org/10.1007/s10570-014-0357-5.

Kumar, V., Pathak, P., Bhardwaj, N.K. (2021) Micro-nanofibrillated cellulose preparation from bleached softwood pulp using chemo-refining approach and its evaluation as strength enhancer for paper properties. Appl. Nanosci. 11:101–115. https://doi.org/10.1007/s13204-020-01575-9.

Lago, C.R., Oliveira, A.L.M., Dias, M.C., Carvalho, E.E.N., Tonoli, G.H.D., Vilas Boas, E.V.B. (2020) Obtaining cellulosic nanofibrils from oat straw for biocomposite reinforcement: Mechanical and barrier properties. Ind. Crop. Prod. 148:112264. https://doi.org/10.1016/j.indcrop.2020.112264.

Li, Q., Wu, Y., Fang, R., Lei, C., Li, Y., Li, Y., Li, B., Pei, Y., Luo, X., Liu, S. (2021) Application of Nanocellulose as particle stabilizer in food Pickering emulsion: Scope, Merits and challenges. Trends Food Sci. Technol., 110:573–583. https://doi.org/10.1016/j.tifs.2021.02.027.

Li, W., Wang, S., Wang, W., Qin, C., Wu, M. (2019) Facile preparation of reactive hydrophobic cellulose nanofibril film for reducing water vapor permeability (WVP) in packaging applications. Cellulose 26:3271–3284. https://doi.org/10.1007/s10570-019-02270-x.

Liang, C., Ruan, K., Zhang, Y., Gu, J. (2020) Multifunctional Flexible Electromagnetic Interference Shielding Silver Nanowires/Cellulose Films with Excellent Thermal Management and Joule Heating Performances. ACS Appl. Mater. Interfaces 12:18023–18031. https://dx.doi.org/10.1021/acsami.0c04482?ref=pdf.

Malucelli, L.C., Matos, M., Jordão, C., Lomonaco, D., Lacerda, L.G., Carvalho Filho, M.A.S., Magalhães, W.L.E. (2019) Influence of cellulose chemical pretreatment on energy consumption and viscosity of produced cellulose nanofibers (CNF) and mechanical properties of nanopapers. Cellulose 26:1667–1681. https://doi.org/10.1007/s10570-018-2161-0.

Martins, C.C.N., Dias, M.C., Mendonça, M.C., Durães, A.F.S., Silva, L.E., Félix, J.R., Damásio, R.A.P., Tonoli, G.H.D. (2021) Optimizing cellulose microfibrillation with NaOH pretreatments for unbleached *Eucalyptus* pulp. Cellulose 28:11519–11531. https://doi.org/10.1007/s10570-021-04221-x.

Mascarenhas, A.R.P., Scatolino, M.V., Santos, A.A., Norcino, L.B., Duarte, P.J., Melo, R.R., Dias, M.C., Faria, C.E.T., Mendonça, M.C., Tonoli, G.H.D. (2022) Hydroxypropyl methylcellulose films reinforced with cellulose micro/nanofibrils: study of physical, optical, surface, barrier and mechanical properties. Nord. Pulp Pap. Res. J. 1–16. https://doi.org/10.1515/npprj-2022-0006.

Melati, R.B., Shimizu, F.L., Oliveira, G., Pagnocca, F.C., Souza, W., Sant'Anna, C., Brienzo, M. (2019) Key Factors Affecting the Recalcitrance and Conversion Process of Biomass. BioEnergy Res. 12:1–20. https://doi.org/10.1007/s12155-018-9941-0.

Moghaddam, M.K., Karimi, E. (2020) The effect of oxidative bleaching treatment on Yucca fiber for potential composite application. Cellulose 27:9383–9396. https://doi.org/10.1007/s10570-020-03433-x.

Mohammed, N., Grishkewich, N., Tam, K.C. (2018) Cellulose nanomaterials: promising sustainable nanomaterials for application in water/wastewater treatment processes. Environ. Sci. Nano. 5:623–658. https://doi.org/10.1039/C7EN01029J.

Mohtaschemi, M., Dimic-Misic, K., Puisto, A., Korhonen, M., Maloney, T., Paltakari, J., Alava, M.J. (2014) Rheological characterization of fibrillated cellulose suspensions via bucket vane viscosimeter. Cellulose 21:1305–1312. https://doi.org/10.1007/s10570-014-0235-1.

Mokhena, T.C., John, M.J. (2020) Cellulose nanomaterials: new generation materials for solving global issues. Cellulose 27:1149–1194. https://doi.org/10.1007/s10570-019-02889-w.

Mokhena, T.C., Sadiku, E.R., Mochane, M.J., Ray, S.S., John, M.J., Mtibe, A. (2021) Mechanical properties of cellulose nanofibril papers and their bionanocomposites: A review. Carbohydr. Polym. 273:118507. https://doi.org/10.1016/j.carbpol.2021.118507.

Moraes, J.O., Scheibe, A.S., Sereno, A., Laurindo, J.B. (2013) Scale-up of the production of cassava starch based films using tape casting. J. Food Eng. 119:800–808. https://doi.org/10.1016/j.jfoodeng.2013.07.009.

Moser, C., Lindström, M.E., Henriksson, G. (2015) Toward Industrially Feasible Methods for Following the Process of Manufacturing Cellulose Nanofibers. BioResources 10:2360–2375. https://doi.org/10.15376/biores.10.2.2360-2375.

Nascimento, E.S., Barros, M.O., Cerqueira, M.A., Lima, H.L., Borges, M.F., Pastrana, L.M., Gama, F.M., Rosa, M.F., Azeredo, H.M.C., Gonçalves, C. (2021) All-cellulose nanocomposite films based on bacterial cellulose nanofibrils and nanocrystals. Food Packag. Shelf Life 29:100715. https://doi.org/10.1016/j.fpsl.2021.100715.

Niu, X., Liu, Y., Fang, G., Huang, C., Rojas, O.J., Pan, H. (2018) Highly Transparent, Strong, and Flexible Films with Modified Cellulose Nanofiber Bearing UV Shielding Property. Biomacromolecules 19:4565–4575. https://doi.org/10.1021/acs.biomac.8b01252.

Noorbakhsh-Soltani, S.M., Zerafat, M.M., Sabbaghi, S. (2018) A comparative study of gelatin and starch-based nano-composite films modified by nano-cellulose and chitosan for food packaging applications. Carbohydr. Polym. 189:48–55. https://doi.org/10.1016/j.carbpol.2018.02.012.

Noremylia, M.B., Hassan, M.Z., Ismail, Z. (2022) Recent advancement in isolation, processing, characterization and applications of emerging nanocellulose: A review. Int. J. Biol. Macromol. 206:954–976. https://doi.org/10.1016/j.ijbiomac.2022.03.064.

Osong, S.H., Norgren, S., Engstrand, P. (2016) Processing of wood-based microfibrillated cellulose and nanofibrillated cellulose, and applications relating to papermaking: a review. Cellulose 23:23–123. https://doi.org/10.1007/s10570-015-0798-5.

Perrin, L., Gillet, G., Gressin, L., Desobry, S. (2020) Interest of pickering emulsions for sustainable micro/nanocellulose in food and cosmetic applications. Polymers 12:2385. https://doi.org/10.3390/polym12102385.

Qaseem, M.F., Shaheen, H., Wu, A.M. (2021) Cell wall hemicellulose for sustainable industrial utilization. Renew. Sustain. Energy Rev. 144:110996. https://doi.org/10.1016/j.rser.2021.110996.

Qu, J., Yuan, Z., Wang, C., Wang, A., Liu, X., Wei, B., Wen, Y. (2019) Enhancing the redispersibility of TEMPO-mediated oxidized cellulose nanofibrils in N,N-dimethylformamide by modification with cetyltrimethylammonium bromide. Cellulose

26:7769–7780. https://doi.org/10.1007/s10570-019-02655-y.
R CORE TEAM (2020). R: A language and environment for statistical computing. https://www.R-project.org/. Acessado 15 dez 2020.
Raj, P., Varanasi, S., Batchelor, W., Garnier, G. (2015) Effect of cationic polyacrylamide on the processing and properties of nanocellulose films. J. Colloid Interface Sci. 447:113–119. https://doi.org/10.1016/j.jcis.2015.01.019.
Rol, F., Banvillet, G., Meyer, V., Petit-Conil, M., Bras, J. (2018) Combination of twin-screw extruder and homogenizer to produce high-quality nanofibrillated cellulose with low energy consumption. Journal of Material. Science 53:12604–12615. https://doi.org/10.1007/s10853-018-2414-1.
Rol, F., Belgacem, M.N., Gandini, A., Bras, J. (2019) Recent advances in surface-modified cellulose nanofibrils. Prog. Polym. Sci. 88:241–264. https://doi.org/10.1016/j.progpolymsci.2018.09.002.
Rueden, C.T., Schindelin, J., Hiner, M.C., Dezonia, B.E., Walter, A.E., Arena, E.T., Eliceiri, K.W. (2017) ImageJ2: ImageJ for the next generation of scientific image data. BMC Bioinform. 18:529. https://doi.org/10.1186/s12859-017-1934-z.
Santucci, B.S., Bras, J., Belgacem, M.N., Curvelo, A.A.S., Pimenta, M.T.B. (2016) Evaluation of the effects of chemical composition and refining treatments on the properties of nanofibrillated cellulose films from sugarcane bagasse. Ind. Crop. Prod. 91:238–248. https://doi.org/10.1016/j.indcrop.2016.07.017.
Shimizu, M., Saito, T., Isogai, A. (2016) Water-resistant and high oxygen-barrier nanocellulose films with interfibrillar cross-linkages formed through multivalent metal ions. J. Membr. Sci. 500:1–7. https://doi.org/10.1016/j.memsci.2015.11.002.
Sothornvit, R., Hong, Si., An, D.J., Rhim, J.W. (2010) Effect of clay content on the physical and antimicrobial properties of whey protein isolate/organo-clay composite films. Lebensm.-Wiss. Technol. 43:279–284. https://doi.org/10.1016/j.lwt.2009.08.010.
Suhag, R., Kumar, N., Petkoska, A.T., Upadhyay, A. (2020) Film formation and deposition methods of edible coating on food products: A review. Food Res. Int. 136:109582. https://doi.org/10.1016/j.foodres.2020.109582.
Sukmawan, R., Kusmono, Rahmanta, A.P., Saputri, L.H. (2022) The effect of repeated alkali pretreatments on the morphological characteristics of cellulose from oil palm empty fruit bunch fiber-reinforced epoxy adhesive composite. Int. J. Adhes. Adhes. 114:103095. https://doi.org/10.1016/j.ijadhadh.2022.103095.
TAPPI Standard (2012) T 559 cm-12, Grease resistance test for paper and paperboard.
TAPPI Standard (2013) T 410 om-08, Grammage of paper and paperboard.
TAPPI Standard (2015) T 411 om-15, Thickness of paper, paperboard, and combined board.
TAPPI Standard (2021a) T 249 cm-21, Carbohydrate composition of extractive-free wood and wood pulp by gas-liquid chromatography.
TAPPI Standard (2021b) T 222 om-21, Acid-soluble lignin in wood and pulp.
TAPPI Standard (2021c) T 402 sp-21, Standard conditioning and testing atmospheres for paper, board, pulp handsheets, and related products.
Tayeb, A.H., Amini, E., Ghasemi, S., Tajvidi, M. (2018) Cellulose Nanomaterials – Binding Properties and Applications: A Review. Molecules 23:2684. http://dx.doi.org/10.3390/molecules23102684.
Teodoro, K.B.R., Sanfelice, R.C., Migliorini, F.L., Pavinatto, A., Facure, M.H.M., Correa, D.S. (2021) A Review on the Role and Performance of Cellulose Nanomaterials in Sensors. ACS Sens. 6:2473–2496. https://doi.org/10.1021/acssensors.1c00473.
Trovagunta, R., Kelley, S.S., Lavoine, N. (2021) Highlights on the mechanical pre-refining step in the production of wood cellulose nanofibrils. Cellulose 28:11329–11344. https://doi.org/10.1007/s10570-021-04226-6.
Turpeinen, T., Jäsberg, A., Haavisto, S., Liukkonen, J., Salmela, J., Koponen, A.I. (2020) Pipe rheology of microfibrillated cellulose suspensions. Cellulose 27:141–156. https://doi.org/10.1007/s10570-019-02784-4.
Tyagi, P., Hubbe, M.A., Lucia, L., Pal, L. (2018) High performance nanocellulose-based composite coatings for oil and grease resistance. Cellulose 25:3377–3391. https://doi.org/10.1007/s10570-018-1810-7.
Verker, R., Grossman, E., Eliaz, N. (2009) Erosion of POSS-polyimide films under hypervelocity impact and atomic oxygen: The role of mechanical properties at elevated temperatures. Acta Mater. 57:1112–1119. https://doi.org/doi:10.1016/j.actamat.2008.10.054.
Wang, J., Gardner, D.J., Stark, N.M., Bousfield, D.W., Tajvidi, M., Cai, Z. (2018) Moisture and Oxygen Barrier Properties of Cellulose Nanomaterial-Based Films. ACS Sustainable Chemistry &. Engineering 6:46–70. https://doi.org/10.1021/acssuschemeng.7b03523.
Wang, L., Chen, C., Wang, J., Gardner, D.J., Tajvidi, M. (2020) Cellulose nanofibrils versus cellulose nanocrystals: Comparison of performance in flexible multilayer films for packaging applications. Food Packag. Shelf Life 23:100464. https://doi.org/10.1016/j.fpsl.2020.100464.
Wang, Q., Zhu, J.Y., Considine, J.M. (2013) Strong and Optically Transparent Films Prepared Using Cellulosic Solid Residue Recovered from Cellulose Nanocrystals Production Waste Stream. ACS Appl. Mater. Interfaces 5:7. https://doi.org/10.1021/am302967m.
Wu, C., McClements, D.V., He, M., Zheng, L., Tian, T., Teng, F., Li, Y. (2021) Preparation and characterization of okara nanocellulose fabricated using sonication or high-pressure homogenization treatments. Carbohydr. Polym. 255:117364. https://doi.org/10.1016/j.carbpol.2020.117364.
Xinping, L., Nan, W., Xin, Z., Hui, C., Yaoyu, W., Zhao, Z. (2020) Optical haze regulation of cellulose nanopaper via morphological tailoring and nano-hybridization of cellulose nanoparticles. Cellulose 27:1315–1326. https://doi.org/10.1007/s10570-019-02876-1.
Yang, X., Berthold, F., Berglund, L.A. (2019a) High-Density Molded Cellulose Fibers and Transparent Biocomposites Based on Oriented Holocellulose. ACS Appl. Mater. Interfaces 11:10310–10319. http://dx.doi.org/10.1021/acsami.8b22134.
Yang, W., Jiao, L., Liu, W., Dai, H. (2019b) Manufacture of Highly Transparent and Hazy Cellulose Nanofibril Films via Coating TEMPO-Oxidized Wood Fibers. Nanomaterials 9:107. https://doi.org/10.3390/nano9010107.
Yook, S., Park, H., Park, H., Lee, S.Y., Kwon, J., Youn, H.J. (2020) Barrier coatings with various types of cellulose nanofibrils

and their barrier properties. Cellulose 27:4509–4523. https://doi.org/10.1007/s10570-020-03061-5.

Zhang, B.X., Azuma, J.I., Uyama, H. (2015) Preparation and characterization of a transparent amorphous cellulose film. RSC Adv. 4:2900. https://doi.org/10.1039/C4RA14090G.

Zhang, W., Zhang, Y., Cao, J., Jiang, W. (2021) Improving the performance of edible food packaging films by using nanocellulose as an additive. Int. J. Biol. Macromol. 166:288–296. https://doi.org/10.1016/j.ijbiomac.2020.10.185.

Zhou, X., Li, W., Mabon, R., Broadbelt, L.J. (2016) A critical review on hemicellulose pyrolysis. Energy Technol. 5:52–79. https://doi.org/10.1002/ente.201600327.

Žepič, V., Fabjan, E.S., Kasunic, M., Korosec, M., Hancic, A., Oven, P., Perse, L.S., Polijansek, I. (2014) Morphological, thermal, and structural aspects of dried and redispersed nanofibrillated cellulose (NFC). Holzforschung 68:657–667. https://doi.org/10.1515/hf-2013-0132.